Available online at www.sciencedirect.com
ScienceDirect
Journal of Catalysis 252 (2007) 215–230
JOURNAL OF CATALYSIS
www.elsevier.com/locate/jcat

Cobalt species in promoted cobalt alumina-supported Fischer–Tropsch catalysts

Wei Chu [a,b], Petr A. Chernavskii [c], Léon Gengembre [a], Galina A. Pankina [c], Pascal Fongarland [a], Andrei Y. Khodakov [a,*]

[a] *Unité de Catalyse et de Chimie du Solide, UMR 8181 CNRS, Bât. C3, USTL-ENSCL-EC Lille, Cite Scientifique, 59655 Villeneuve d'Ascq, France*
[b] *Department of Chemical Engineering, Sichuan University, Chengdu 610065, China*
[c] *Department of Chemistry, Moscow State University, 119992 Moscow, Russia*

Received 11 July 2007; revised 23 September 2007; accepted 24 September 2007

Available online 26 October 2007

Abstract

The structure of cobalt species at different stages of the genesis of monometallic and Pt-promoted cobalt alumina-supported Fischer–Tropsch catalysts was studied using X-ray diffraction, UV–visible spectroscopy, in situ X-ray absorption, in situ magnetic method, X-ray photoelectron spectroscopy, and DSC–TGA thermal analysis. The catalysts were prepared by incipient wetness impregnation using solutions of cobalt nitrate and dihydrogen hexachloroplatinate. Both variation of catalyst calcination temperature between 473 and 773 K and promotion with 0.1 wt% of Pt had no significant affect on the size of supported Co_3O_4 crystallites. The size of cobalt oxide particles in the calcined catalysts seems to be influenced primarily by the pore diameter of the support. Cobalt reducibility was relatively low in monometallic cobalt alumina-supported catalysts and decreased as a function of catalyst calcination temperature. The effect was probably due to the formation of mixed surface compounds between Co_3O_4 and Al_2O_3 at higher calcination temperatures, which hinder cobalt reduction. Promotion with platinum spectacularly increased the rate of cobalt reduction; the promotion seemed to reduce the activation energy of the formation of cobalt metallic phases. Analysis of the magnetization data suggests that the presence of Pt led to the reduction of smaller cobalt oxide particles, which could not be reduced at the same conditions in the cobalt monometallic catalysts. Promotion of cobalt alumina-supported catalysts with small amounts of Pt resulted in a significant increase in Fischer–Tropsch cobalt time yield. The efficient control of cobalt reducibility through catalyst calcination and promotion seems to be one of the key issues in the design of efficient cobalt alumina-supported Fischer–Tropsch catalysts.

Keywords: Clean fuels; Fischer–Tropsch synthesis; Nanoparticles; Catalyst preparation; Alumina; Cobalt catalyst; Promotion; Dispersion; Reducibility; In situ X-ray absorption; XANES; EXAFS; In situ magnetic method

1. Introduction

In the twenty-first century, natural gas is expected to become an increasingly important raw material for manufacturing clean fuels and chemicals [1–3]. Fischer–Tropsch (FT) synthesis is a major part of gas-to-liquids (GTL) technology, which converts natural gas into liquid fuels with very low sulfur and aromatic content [1–4]. Production of syngas from methane, coal, and biomass followed by subsequent conversion of syngas to a wide range of fuels and chemicals is of particular interest as the worldwide reserves of crude oil are being depleted.

Cobalt catalysts have been used for FT synthesis, because they are efficient in manufacturing long-chain normal paraffins and they exhibit high resistance to deactivation [2,5–7]. Significant efforts have focused on the optimization and tailoring of cobalt catalysts for specific applications. It has been demonstrated that cobalt active component, support, and promoter have important effects on the catalyst performance and structure. On the one hand, Iglesia et al. [5–7] reported that for relatively large cobalt particles ($d > 10$ nm), FT reac-

* Corresponding author. Mailing address for correspondence: Unité de Catalyse et de Chimie du Solide, Université des Sciences et Technologies de Lille, Bât. C3, Cité Scientifique, 59655 Villeneuve d'Ascq, France. Fax: +33 3 20 43 65 61.
E-mail address: andrei.khodakov@univ-lille1.fr (A.Y. Khodakov).

0021-9517/$ – see front matter
doi:10.1016/j.jcat.2007.09.018

tion rates were proportional to metal dispersion. On the other hand, Bartholomew [8], Kuznetsov, Yermakov [9,10], and de Jong [11] observed lower FT turnover frequencies with cobalt particles smaller than 6–8 nm. It seems that lower activity of small cobalt particles might be attributed to both their reoxidation at the reaction conditions and modified electronic structure because of the quantum size effect. A recent report by van de Loosdrecht et al. [12] reinforces that currently there is no consistent picture regarding oxidation of cobalt particles during FT reaction. It was shown that reoxidation of cobalt metal particles in industrial FT reactors could be prevented by efficient control of water and hydrogen pressures. Thus, the observed decrease in FT productivity during the reaction likely cannot be assigned solely to cobalt particle oxidation. Analysis of the literature [2] suggests that a highly active cobalt catalyst would require optimal-sized of cobalt metal particles, high reducibility, and high stability of cobalt active sites.

Thus, both catalyst promotion and different pretreatments seem to be helpful in mastering efficient cobalt FT catalysts. Numerous studies have shown that promotion of cobalt FT catalysts with noble metals (Ru, Rh, Pt, and Pd) has a significant impact on the structure and dispersion of cobalt species, FT reaction rates, and selectivities. The promotion of cobalt FT catalysts with noble metals has been reviewed previously [2,13].

Besides the promotion, the structure and catalytic properties of cobalt catalysts also can be controlled by oxidative pretreatments. We have addressed the effect of oxidative pretreatments on the structure of cobalt silica-supported catalysts in previous reports [14–16]. We found that lower temperature of decomposition of cobalt precursor and lower calcination temperature improve cobalt dispersion. Lower pretreatment temperature results in higher number of cobalt active sites and thus, better catalytic performance. The presence of catalyst promoter (noble metal or sucrose [16,17]) also can affect cobalt nitrate decomposition and modify cobalt dispersion, catalyst structure, and catalytic performance.

It is known that several parameters of catalyst calcination can influence the performance of cobalt FT catalysts. The benefits of direct reduction of cobalt nitrate on cobalt dispersion have been reported by Iglesia [5,18]. Enache et al. [19] found that direct reduction of cobalt nitrate produced more active Co/Al_2O_3 catalyst, whereas catalyst calcination led to Co_3O_4 crystallites, which were more difficult to reduce. Van de Loosdrecht et al. [20] showed that the use of rotary kilns, different furnaces, and fluidized reactors influenced the properties of cobalt alumina catalysts. The gas flow rate during catalyst calcination also has a significant impact on the sizes of cobalt oxide crystallites: the greater the flow rate, the smaller the Co_3O_4 crystallites [20]. De Jong and coworkers [21,22] have shown that changing the gas atmosphere from air to 1% NO/He during thermal treatment of supported Ni-nitrate or Co-nitrate delivers improved metal oxide dispersion. In a very recent report, Borg et al. [23] proposed that low calcination temperature and efficient removal of the precursor decomposition products can be essential to maximizing cobalt dispersion in cobalt catalysts supported on γ-alumina. The variation in the sizes of cobalt oxide crystallites evaluated from the Scherrer broadening of XRD patterns was relatively small (between 9.6 and 12.3 nm), however.

The present paper addresses the effects of catalyst calcination temperature and platinum promotion on the structure of monometallic and Pt-promoted alumina-supported cobalt FT catalysts and on the interaction between the Co_3O_4 crystallites and alumina support. A wide range of methods was used for catalyst characterization, including X-ray diffraction (XRD), temperature-programmed reduction (TPR), X-ray photoelectron spectroscopy, in situ X-ray absorption spectroscopy (XANES and EXAFS), and in situ magnetic method. The catalytic performance in FT synthesis was evaluated in a fixed-bed microreactor.

2. Experimental

2.1. Catalysts

The alumina-supported cobalt monometallic catalysts were prepared by conventional incipient wetness impregnation of γ-alumina using aqueous solutions of cobalt nitrate. The cobalt catalysts promoted with platinum were prepared by co-impregnation using aqueous solutions containing cobalt nitrate and dihydrogen hexachloroplatinate. Commercial Puralox SCCA-5/170 alumina (Sasol), with $S_{BET} = 165\ m^2/g$, pore diameter of 8.3 nm, and total pore volume of $0.477\ cm^3/g$, was used as a catalytic support. After the impregnation or co-impregnation, the catalyst samples (ca. 10 g) were dried at 373 K in an oven, then calcined in air flow of 120 cm^3/min at 473, 613, 673, and 773 K for 10 h (Table 1). The catalysts prepared without and with platinum addition are designated "Co/Al_2O_3-Temp" and "$CoPt/Al_2O_3$-Temp," where "Pt" indicates Pt addition and "Temp" indicates the temperature of calcination.

The catalysts were reduced in a flow of hydrogen at 673 K for 5 h. The temperature ramping rate was 3 K/min.

2.2. X-ray diffraction

Powder XRD patterns were recorded by a Siemens D5000 diffractometer using Cu($K\alpha$) radiation. The average crystallite size of Co_3O_4 was calculated using both 422 ($2\theta = 56.0°$) and

Table 1
Preparation and chemical composition of cobalt alumina-supported catalysts

Catalyst symbol	Co content (wt%)	Pt content (wt%)	Calcination temperature, K	Co_3O_4 particle size (nm), XRD
Co/Al_2O_3	15	–	Drying at 363	–
Co/Al_2O_3-473	15	–	473	9.5
Co/Al_2O_3-613	15	–	613	9.0
Co/Al_2O_3-673	15	–	673	9.9
Co/Al_2O_3-773	15	–	773	9.6
$CoPt/Al_2O_3$	15	0.1	Drying at 363	–
$CoPt/Al_2O_3$-473	15	0.1	473	9.3
$CoPt/Al_2O_3$-613	15	0.1	613	9.2
$CoPt/Al_2O_3$-673	15	0.1	673	9.0
$CoPt/Al_2O_3$-773	15	0.1	773	9.6

511 ($2\theta = 59.5°$) diffraction lines according to Scherrer's equation [24].

2.3. DSC–TGA

Simultaneous differential scanning calorimetry and thermogravimetric analysis were carried out in a flow of air at temperature rate of 2 K/min using DSC–TGA SDT 2960 thermal analyzer. The sample loading was typically 25–30 mg.

2.4. X-ray absorption

The X-ray absorption spectra at the Co K-edge were measured at the European Synchrotron Radiation Facility (DUBBLE-CRG, Grenoble, France) using an in situ X-ray absorption cell as described previously [25]. The measurements were performed in transmission mode, with two ionization chambers used for X-ray detection. The Si(111) double-crystal monochromator was calibrated by setting the first inflection point of the K-edge spectrum of the Co foil at 7709 eV. Measuring an X-ray absorption spectrum (7600–8400 eV) took about 30–40 min. The X-ray absorption data were analyzed using the conventional procedure. After background correction, the XANES spectra were normalized by the edge height. After subtraction of the metal atomic absorption, the k^2-weighted EXAFS signal was transformed without phase correction from k space to r space to obtain the radial distribution function. Crystalline Co_3O_4, CoO, and Co foil were used as reference compounds for XANES and EXAFS analysis.

2.5. XPS

Surface analyses were performed with a VG ESCALAB 220XL spectrometer. The Al$K\alpha$ monochromatized line (1486.6 eV) was used for excitation with 300-W of applied power. The analyzer was operated in a constant pass energy mode ($E_{pass} = 40$ eV). Binding energies were referenced to the Al 2p core level (74.6 eV) of the Al_2O_3 support. The reproducibility was ±0.2 eV for Co 2p binding energy. The experimental Co 2p XPS spectra of the catalysts were normalized by the intensity of the Al 2p line. To avoid calibration problems due to the XPS spectrometer, the $2p_{1/2}$–$2p_{3/2}$ spin–orbital splittings and intensity of satellite structures were used along with the absolute values of Co 2p binding energies for the analysis of XPS data. The vacuum level during the experiment was $>10^{-7}$ Pa. The powdered catalyst was pressed into a thin pellet onto a steel block. In situ reduction was carried out in pure hydrogen at 673 K for 5 h in the reactor cell of the preparation chamber attached to the analysis chamber of the spectrometer. Then the reduced sample was transferred to the analysis chamber of the spectrometer under vacuum without exposure to air. The pressure in the XPS preparation chamber during the transfer was about 10^{-6} Pa.

2.6. In situ magnetic measurements

The in situ magnetic measurements were performed using a Foner vibrating-sample magnetometer described previously [26,27]. The design of the magnetometer allows the recording of curves of magnetization during temperature-programmed heating or under isothermal conditions at 280–973 K temperature range. The temperature-programmed reduction experiments were carried out in pure hydrogen. The amount of samples was about 30 mg. The gas flow velocity was 30 cm^3/min. The appearance of cobalt metallic species in the catalysts was monitored in situ by continuous increase in sample magnetization during the reduction.

For the evaluation of cobalt metal particle sizes from magnetic data, the catalysts were first reduced in a flow of hydrogen. After attaining the constant value of magnetization at a given temperature, the catalyst sample is cooled down to 473 K. The hydrogen flow was replaced by argon at 473 K to desorb hydrogen species from the catalyst. Then the sample was cooled down in argon to 280 K. The dependencies of magnetization on the intensity of magnetic field (field dependences) were measured at 280 K by scanning the intensity of the magnetic field to 6.2 kOe. The saturation magnetization (J_s) was measured by extrapolation in the coordinates J of versus $1/H$, where J was the sample magnetization and H was the intensity of magnetic field. The mild low-temperature oxidation of the reduced cobalt catalyst was performed in 1% O_2/He mixture at 280 K. The coercive force was measured before and after the oxidation.

2.7. Catalytic measurements

The FT synthesis was carried out in a fixed-bed stainless steel reactor (9 mm i.d.) with plug-flow hydrodynamics operating at 1 bar and 443–483 K. The thermocouple was in direct contact with the catalyst. The design permitted measurement of temperature along the catalyst bed; no heat spot was detected during the FT synthesis. Typically the gas hourly space velocity of 1800 $cm^3/g/h$ at STP and a H_2/CO molar ratio of 2 were used. Carbon monoxide contained 5% N_2, which was used as an internal standard. The gas flow rates for reactant gases were controlled by mass flow controllers (Brooks). At each specified experimental conditions the catalytic measurements were carried out for at least 24 h; the steady-state conditions were normally attained within 5 h of the reaction. The reactant gases and hydrocarbon products were analyzed by gas chromatography (Hewlett-Packard 5890) with respectively a thermal conductivity detector and a flame ionization detector. To avoid possible condensation of the reaction products, the gas transfer lines were constantly heated at 423 K. Analysis of H_2, CO, CO_2, and CH_4 was performed with a 13X molecular sieve column and a thermal conductivity detector. Hydrocarbons (C1–C20) were separated in 10% CP-Sil5 on a Chromosorb WHP packed column and analyzed with a flame-ionization detector. The hydrocarbon selectivities were calculated on carbon basis.

3. Results

3.1. Cobalt species in oxidized catalysts

Impregnated and dried cobalt monometallic catalyst (Co/Al_2O_3-363 in Table 2) exhibits the XPS spectrum shown in

Table 2
XPS data for calcined catalysts

Catalyst	Major cobalt phase	Co 2p binding energy, eV	Spin–orbital splitting, eV	Atomic ratio n_{Co}/n_{Al}	Atomic ratio n_N/n_{Co}
Co/Al_2O_3-363	Co^{2+}	781.5	15.9	0.74	0.74
Co/Al_2O_3-473	Co_3O_4	780.8	15.2	0.14	0.44
$CoPt/Al_2O_3$-473	Co_3O_4	780.8	15.2	0.13	0.65
Co/Al_2O_3-613	Co_3O_4	781.2	15.2	0.18	–
$CoPt/Al_2O_3$-613	Co_3O_4	780.9	15.2	0.18	–
Co/Al_2O_3-673	Co_3O_4	780.9	15.5	0.13	–
Co/Al_2O_3-773	Co_3O_4	780.9	15.5	0.26	–

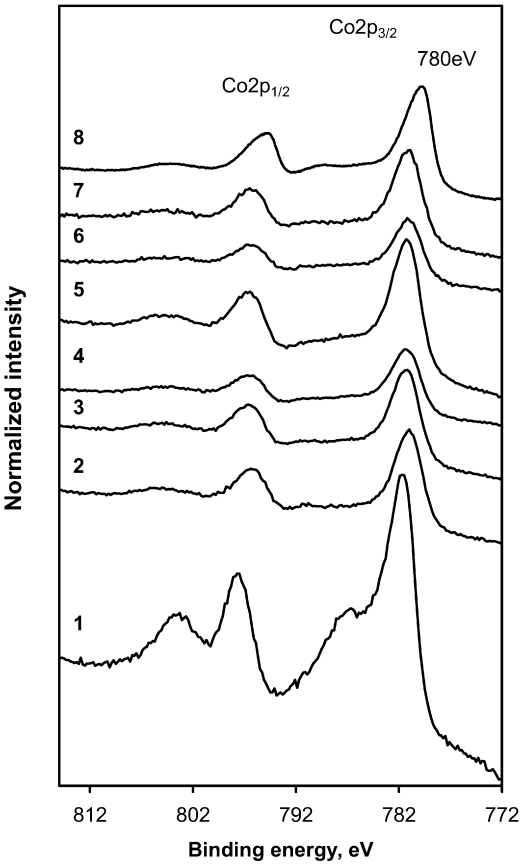

Fig. 1. Co 2p XPS spectra of oxidized Co/Al_2O_3 and $CoPt/Al_2O_3$ catalysts: (1) impregnated and dried Co/Al_2O_3, (2) Co/Al_2O_3-473, (3) Co/Al_2O_3-643, (4) Co/Al_2O_3-673, (5) Co/Al_2O_3-773, (6) $CoPt/Al_2O_3$-473, (7) $CoPt/Al_2O_3$-643, (8) Co_3O_4.

Fig. 1 (curve 1). The observed Co $2p_{1/2}$ and Co $2p_{3/2}$ peaks with binding energies of 781.5 eV and intense satellite structure [28,29] are characteristic of Co^{2+} species. In addition, impregnated and dried sample has a bright-pink color, which is also indicative of Co^{2+} ions in octahedral coordination. A high surface Co/Al ratio (0.74) measured by XPS (Table 2) suggests rather uniform repartition of Co^{2+} on alumina surface. Detection of nitrogen atoms by XPS in the impregnated and dried Co/Al_2O_3 supposes ($n_N/n_{Co} = 0.736$, Table 2) the presence of undecomposed cobalt nitrate.

The XPS data obtained for impregnated and dried catalysts are consistent with XANES and EXAFS results (Fig. 2). The XANES spectra and Fourier transform of EXAFS of impregnated and dried cobalt monometallic catalyst are almost identical to those of the reference cobalt nitrate compound [$Co(NO_3)_2{\cdot}6H_2O$]. This supposes that in the impregnated and dried catalysts, cobalt has octahedral coordination and cobalt electronic state is very similar to that in cobalt nitrate. Note that the EXAFS did not show the presence of cobalt atoms in the second coordination sphere of cobalt (Fig. 2b). This is indicative of mononuclearity of supported cobalt complexes.

After impregnation and drying, the catalysts were calcined in a flow of air. Fig. 3 displays TGA and DSC curves in air of both monometallic and Pt-promoted alumina-supported catalysts. The weight loss curves for both impregnated and dried Co/Al_2O_3 and $CoPt/Al_2O_3$ exhibited several inflections at 323–473 K, due to the endothermic loss of water molecules in the cobalt hydrate shell and subsequent decomposition of the nitrate anions. The Co/Al_2O_3 catalyst showed a slightly higher weight loss than $CoPt/Al_2O_3$, possibly due to the greater extent of hydration (Fig. 3a). The heat flow data confirm that decomposition of cobalt nitrate is endothermic. Similar to silica-supported cobalt catalysts, the decomposition of supported cobalt nitrate on alumina proceeds at 423 K. It is known [14,30] that the decomposition of cobalt nitrate leads to the release of nitrogen dioxide, water, and oxygen:

$$3Co(NO_3)_2{\cdot}6H_2O \rightarrow Co_3O_4 + 6NO_2 + O_2 + 18H_2O.$$

Interestingly, promotion with Pt does not seem to affect the decomposition of supported cobalt nitrate to any noticeable degree (Fig. 3).

Fig. 4 displays XRD patterns of cobalt catalysts calcined at temperatures ranging from 473 to 773 K. The patterns are almost identical for both monometallic and Pt-promoted cobalt catalysts, exhibiting the characteristic peaks of γ-alumina and Co_3O_4. Calcination using Scherrer's equation and both 422 ($2\theta = 56.0°$) and 511 ($2\theta = 59.5°$) Co_3O_4 diffraction lines [31,32] yielded crystallites of about 9–10 nm in both calcined monometallic and Pt-promoted cobalt catalysts (Table 1). Thus, catalyst calcination temperature does not seem to produce any noticeable impact on the size of supported Co_3O_4 crystallites. Promotion with platinum also had little affect on the crystallite size of supported cobalt oxide.

The XANES spectra and Fourier transform moduli of calcined Co/Al_2O_3-613 and $CoPt/Al_2O_3$-613 were almost identical to those of the Co_3O_4 reference compounds (Fig. 2). XANES derivative spectra of the oxidized catalysts also matched those of Co_3O_4. Thus, the XAS data also confirm that Co_3O_4 is dominant phase in both calcined monometallic and Pt-promoted cobalt catalysts.

The XPS data (Fig. 1) were consistent with the XAS data. Co_3O_4 was the dominant phase in the calcined catalysts. It was identified by the binding energies, peak shape, spin–orbital splitting of 15.2 eV, and absence of intense satellite structure [29,33,34]. The increase in spin–orbital splitting from 15.2 to 15.5 eV in the samples calcined at 673 and 773 K (Table 2) indicates the presence of Co^{2+} ions and possible formation of cobalt aluminates [35]. In the catalysts calcined at temperatures above 473 K, XPS did not detect residual nitrogen atoms. The

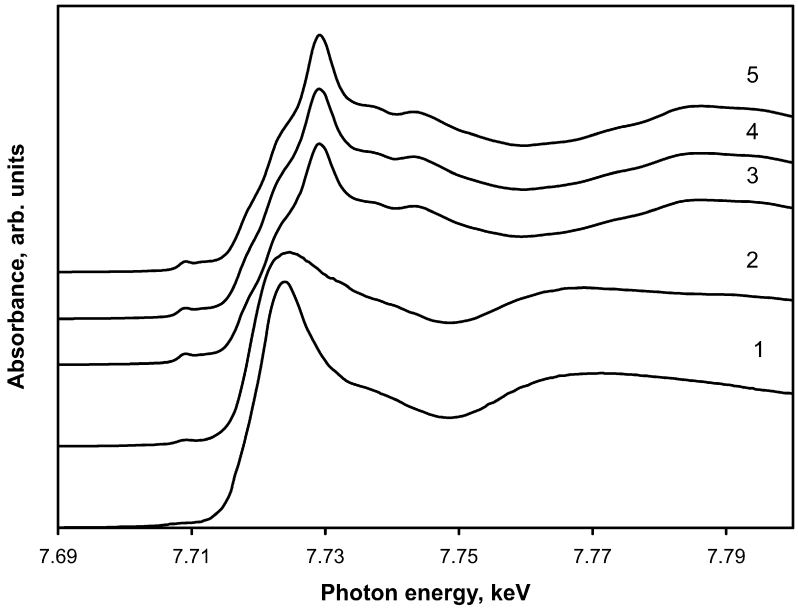

(a)

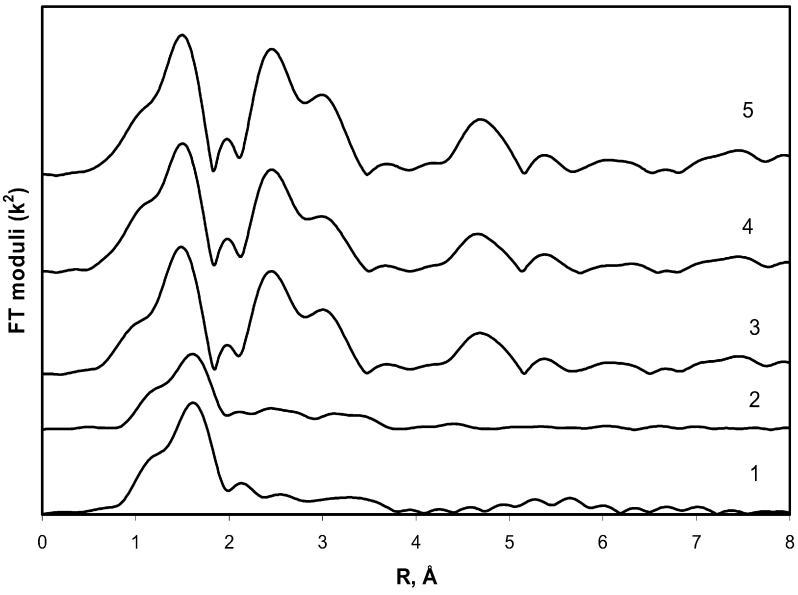

(b)

Fig. 2. XANES spectra and k^2-weighted EXAFS Fourier transform moduli for oxidized monometallic and Pt-promoted cobalt alumina-supported catalysts: (1) $Co(NO_3)_2{\cdot}6H_2O$, (2) Co/Al_2O_3-impregnated and dried, (3) Co/Al_2O_3-613, (4) $CoPt/Al_2O_3$-613, (5) Co_3O_4.

presence of nitrogen may indicate incomplete decomposition of cobalt nitrate. Note, however, that XPS might not be sensitive to low levels of nitrate on an essentially Co_3O_4/Al_2O_3 catalyst.

XPS Co/Al atomic ratios provide information about dispersion of cobalt oxide in the calcined catalysts. Table 2 shows that decomposition of cobalt nitrate and calcination resulted in a dramatic decrease in the Co/Al ratio, from 0.76 in the impregnated and dried catalyst to 0.14 in the calcined catalyst. Interestingly, the CoAl ratio did not much depend on the temperature of catalyst calcination. This suggests that calcination at temperatures below 773 K did not lead to cobalt sintering. Promotion with Pt did not modify the Co/Al ratio in the calcined catalysts (Table 2). In agreement with XRD data, this suggests only very slight effects of calcination temperature and promotion with Pt on the dispersion of cobalt oxide in alumina-supported catalysts.

3.2. Reduction of cobalt catalysts

The TPR profiles of monometallic and promoted cobalt catalysts calcined at different temperatures are shown in Figs. 5 and 6. Several hydrogen consumption peaks can be seen in the TPR curves of cobalt monometallic catalysts. In agreement with previous reports [36–40], low-temperature peaks at 473–573 K can be attributed to partial reduction of Co_3O_4 to CoO,

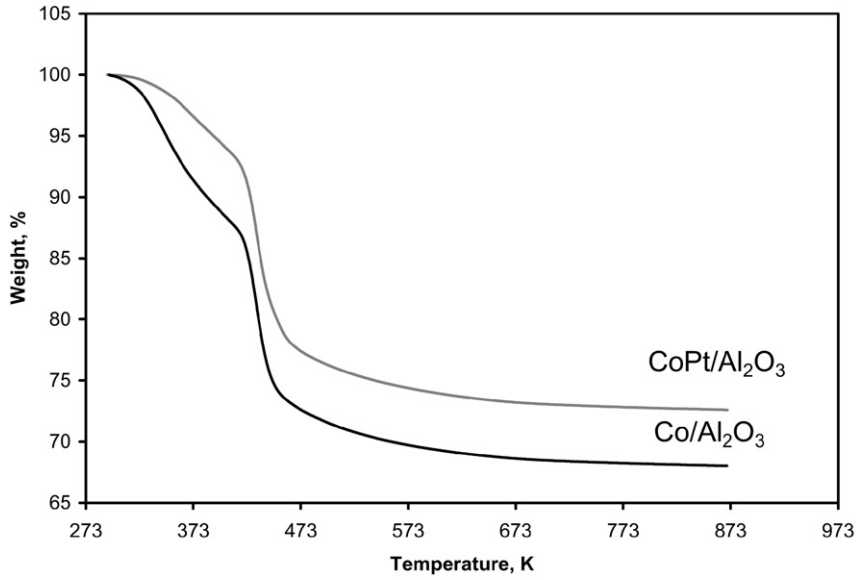

(a)

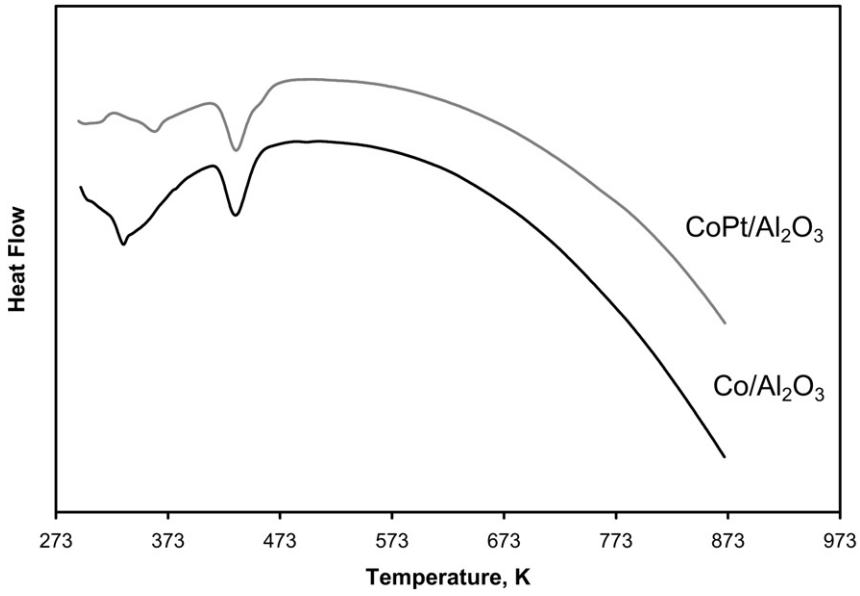

(b)

Fig. 3. TGA (a) and DSC (b) curves of impregnated and dried Co/Al_2O_3 and $CoPt/Al_2O_3$ catalysts. The DSC curves are offset for clarity. Temperature ramp 2 K/min.

whereas high-temperature peaks at 673–773 K are assigned to the reduction of CoO to the cobalt metallic phase. The peaks at 473 K observed in the TPR profile of Co/Al_2O_3-473 likely are attributed either to the reductive decomposition of residual cobalt nitrate [23] or the reduction of CoO(OH) species, as suggested by van de Loosdrecht and van Berge [20,41]. An intense and narrow TPR peak at 480 K in the profile of the $CoPt/Al_2O_3$-473 catalyst (Fig. 6) is likely attributed to the decomposition of cobalt nitrate; it has been reported for other impregnated and dried Co/Al_2O_3 samples containing undecomposed cobalt nitrate.

The position of reduction peaks was found to depend on the catalyst calcination temperature. Reduction of cobalt oxide species was more difficult in the monometallic cobalt catalysts, which were calcined at higher temperatures. In agreement with previous reports, promotion with platinum resulted in a lower-temperature shift of the peaks of reduction of CoO to metallic cobalt (Fig. 6). Interestingly, Pt promotion enhanced both cobalt reduction steps: $Co_3O_4 \rightarrow CoO$ and $CoO \rightarrow Co$.

Note that TPR experiments were conducted in $5\%H_2/Ar$ mixtures, whereas the catalysts were reduced in pure hydrogen for catalytic measurements. It has been shown [27] that hydrogen partial pressure can affect the extent of cobalt reduction. Greater cobalt reduction is usually obtained in pure hydrogen. Thus, TPR measurements provide only qualitative information on cobalt reducibility and cannot be used for quantitative evaluation of the fraction of cobalt metal phase in catalysts reduced in pure hydrogen.

Further information on the reducibility of cobalt species in monometallic and Pt-promoted cobalt catalysts can be derived from the magnetic measurements, which were conducted while heating the catalysts in hydrogen at a linear temperature rate (Fig. 7). The magnetic method is selectively sensitive to the presence of cobalt metal phases [27]. Fig. 7a shows that the temperature of emergence of cobalt metal phase (Table 3) in monometallic cobalt alumina-supported catalysts was a function of catalyst calcination temperature. Cobalt metallic phase was detected in the Co/Al_2O_3-473 catalyst starting at 547 K, whereas in the catalysts precalcined at higher temperature (643, 673, and 773 K), cobalt metallic phase emerged at 570–581 K. Small variations in the temperature of emergence of cobalt metallic phase in these samples (between 570 and 581 K) is probably related to a slightly different distribution of cobalt oxide particle sizes. Both the TPR and magnetic measurements suggest that higher calcination temperature resulted in higher temperatures of genesis of cobalt metal phases. Possible isomorphous substitution of Co^{3+} ions in Co_3O_4 spinel structure by Al^{3+} ions could be one of the reasons for the more difficult reducibility of cobalt catalysts calcined at higher temperatures.

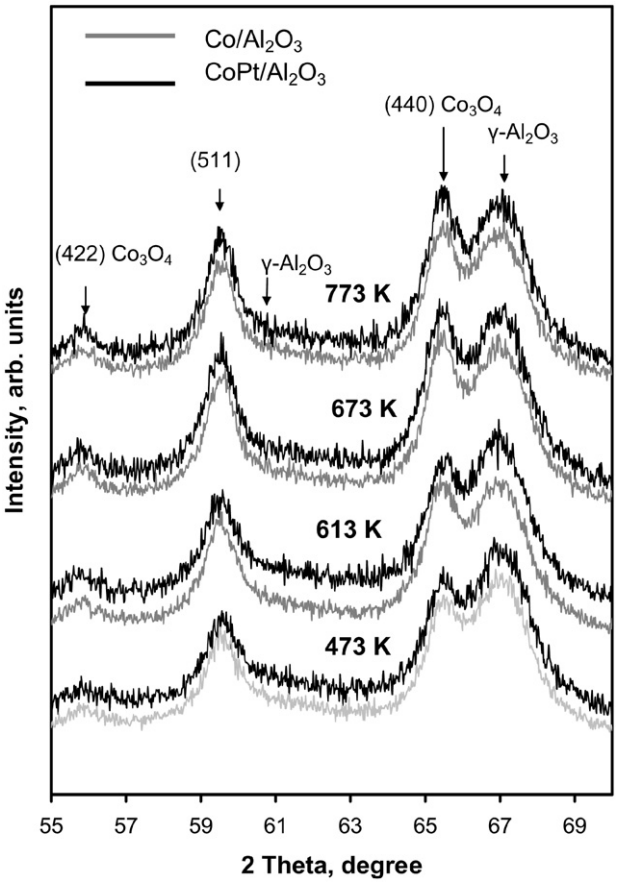

Fig. 4. XRD patterns of cobalt monometallic and Pt-promoted alumina-supported catalysts which were calcined at different temperatures.

Promotion with platinum resulted in a much easier reduction of cobalt oxide to cobalt metal particles (Fig. 7; Table 3). Cobalt metal particles in Pt-promoted catalysts were detected by the magnetic method at 463–473 K, whereas in monometallic cobalt catalysts, the metallic particles were usually observed at 563 K. This is also qualitatively consistent with the TPR results.

Fig. 8 displays differential magnetization (dJ/dT) measured at different heating rates for Co/Al_2O_3-773 and $CoPt/Al_2O_3$-773 catalysts. The maximum of differential magnetization corresponds to an inflection point in the dependence of overall magnetization (J) on temperature (T) (Fig. 7). Thus, differential magnetization is proportional to the rate of formation of cobalt metal phases. Fig. 8 shows that the position of the differential magnetization peaks is a function of catalyst heating rate; the maximum of differential magnetization is situated at lower

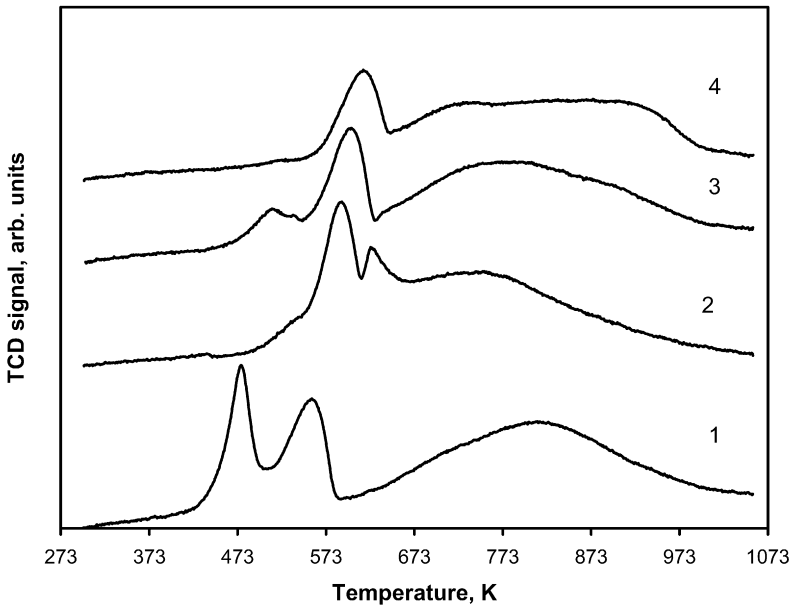

Fig. 5. TPR profiles of monometallic cobalt alumina-supported catalysts calcined at different temperatures: (1) Co/Al_2O_3-473, (2) Co/Al_2O_3-613, (3) Co/Al_2O_3-673, (4) Co/Al_2O_3-773 (5%H_2/Ar mixture, ramping rate 3 K/min).

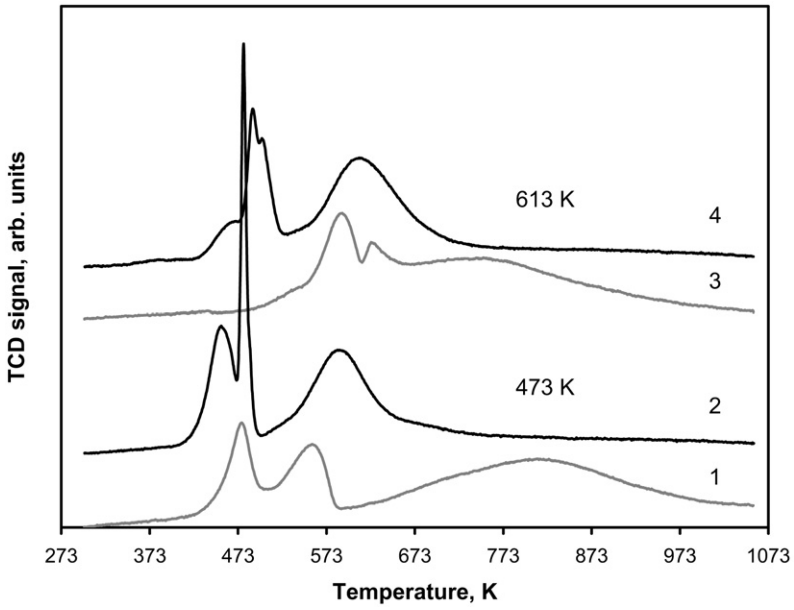

Fig. 6. Effect of promotion with Pt on the TPR profiles of cobalt alumina-supported catalysts: (1) Co/Al_2O_3-473, (2) $CoPt/Al_2O_3$-473, (3) Co/Al_2O_3-613, (4) $CoPt/Al_2O_3$-613 (5%H_2/Ar mixture, ramping rate 3 K/min).

temperature when the catalyst is heated at a slower rate. This suggests that formation of cobalt metal phases is an activated process. Kissinger proposed a method [42] for calculating the activation energy from differential thermal analysis using variation of the maximum of the reaction rate as a function of heating rate. Note that this method of calculating activation energy can be applied to the reactions of any kinetic order. The activation energy of formation of cobalt metal phase can be calculated from the following equation [42]:

$$\frac{\mathrm{d}(\ln \frac{\Phi}{T_\mathrm{m}^2})}{\mathrm{d}(\frac{1}{T_\mathrm{m}})} = -\frac{E}{R},$$

where E is activation energy, R is universal gas constant, Φ is heating rate, and T_m is temperature of maximum of differential magnetization. The activation energy was calculated from the slop in the plot of $\ln(\frac{\Phi}{T_\mathrm{m}^2})$ versus $(\frac{1}{T_\mathrm{m}})$. The activation energies of formation of cobalt metal phases for the Co/Al_2O_3-773 and $CoPt/Al_2O_3$-773 catalysts were 130 and 60 kJ/mol, respectively. Thus, it appears that the promotion of cobalt alumina-supported catalysts with Pt led to a significant drop in the activation energy of cobalt reduction to the metallic phases. The fact that formation of cobalt metal particles is an activated process is consistent with data reported by Bartholomew [43].

3.3. Cobalt species in the reduced catalysts

The XPS spectra of Co/Al_2O_3 and $CoPt/Al_2O_3$ catalysts reduced at 673 K are shown in Fig. 9. Heating under hydrogen resulted in the reduction of supported Co_3O_4 particles to Co^{2+} and cobalt metallic species. Cobalt metallic species were identified using the Co $2p_{3/2}$ peak at 777.9 eV and the Co $2p_{1/2}$ peak at 793–794 eV [37,44]. Oxidized Co^{2+} species were detected by XPS peaks at 781 and 797 eV and an intense satellite structure [28,29]. In monometallic catalysts (Fig. 9, curves 1 and 2), very low concentration of cobalt metallic phases was observed after the treatment with hydrogen at 673 K, whereas both cobalt metallic and Co^{2+} species were detected in Pt-promoted Co/Al_2O_3 catalysts (Fig. 9, curves 3 and 4). This suggests that cobalt reducibility in the alumina-supported catalyst was strongly affected by the presence of platinum. The fraction of Co^{2+} ions and cobalt metal species in the reduced catalysts was evaluated using decomposition of XPS spectra, as we described previously [14]. The Co^0 fractions were 40% for $CoPt/Al_2O_3$-613 and 55% for $CoPt/Al_2O_3$-473.

The XPS data for the reduced catalysts are consistent with X-ray absorption results. The relevant XANES spectra and EXAFS Fourier transform moduli are displayed in Fig. 10. The ref-

Table 3
Characterization of cobalt species in the reduced catalysts using the magnetic method

Catalyst	Temperature of emergence of cobalt metal phase,[a] K	Reduction temperature, K	Fraction of super-paramagnetic cobalt metal particles in the reduced catalysts ($d < 7$ nm), %
Co/Al_2O_3-473	547	973	70
		673	66
Co/Al_2O_3-613	570	973	61
		673	60
Co/Al_2O_3-673	581	973	58
		673	54
Co/Al_2O_3-773	573	973	62
		673	56
$CoPt/Al_2O_3$-473	470	973	87
		673	90
$CoPt/Al_2O_3$-773	486	973	71
		673	77

[a] Reduction in pure hydrogen, ramp 28.2 K/min.

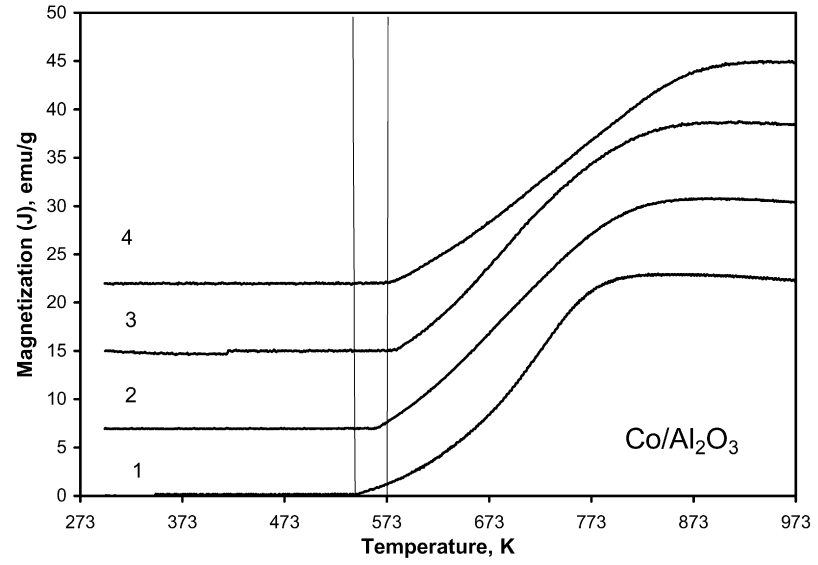

(a)

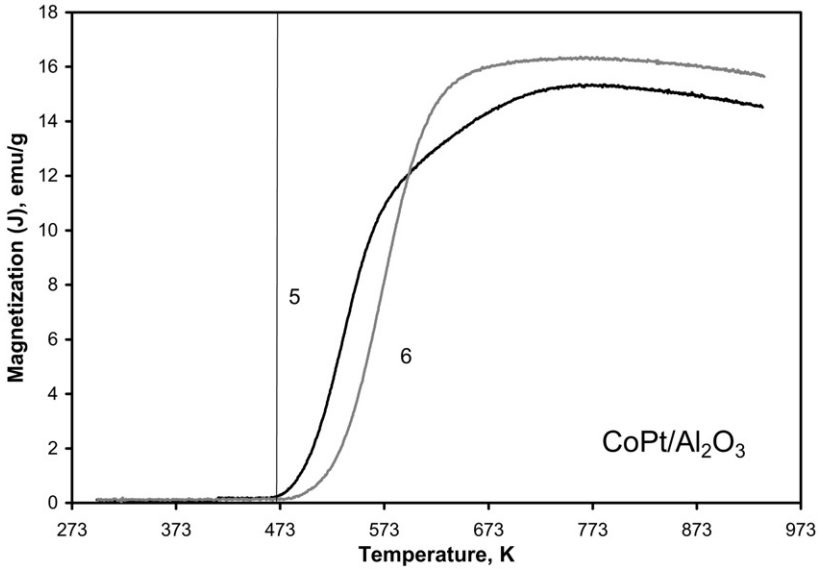

(b)

Fig. 7. Magnetization versus temperature in pure hydrogen for monometallic (a) and Pt-promoted (b) cobalt alumina-supported catalysts calcined at different temperatures: (1) Co/Al_2O_3-473, (2) Co/Al_2O_3-613, (3) Co/Al_2O_3-673, (4) Co/Al_2O_3-773, (5) $CoPt/Al_2O_3$-473, (6) $CoPt/Al_2O_3$-773 (ramping rate 28.2 K/min).

erence data for CoO and Co foil are also shown for comparison. In agreement with XPS data, no noticeable fraction of cobalt metallic phases was observed in the "reduced" Co/Al_2O_3-613. In the reduced $CoPt/Al_2O_3$-613 catalyst, the X-ray absorption data suggest the presence of Co metallic phases.

The sizes of cobalt metal particles in the reduced catalysts were evaluated using the in situ magnetic method. More information about magnetic properties of cobalt compounds and the magnetic method is available in previous reports [26,27].

Two types of particle size analysis were performed. The preliminary analysis was performed using variation of coercive force during mild oxidation. The coercive force or coercivity is the force required to remove the residual magnetism from the material. The coercive force of small superparamagnetic particles is equal to zero. The coercive force increases with higher fraction of single-domain ferromagnetic particles in the catalysts. It is known that the dependence of coercive force on the particle size exhibits a maximum [45]. For cobalt, a maximum of coercive force corresponds to a size of ∼20 nm, which is characteristic of the upper limit of single-domain ferromagnetic cobalt particles [45]. The coercive force decreases with increasing the sizes of multi-domain cobalt particles attaining the limiting value of bulk metal. Low-temperature oxidation of metals ($T < 600$ K) usually proceeds through formation of thin oxide films on the surface of metal particles [46]. The kinetics of growth of these films can be described by the Cabrera–Mott theory [47]. The mechanism of metal particle oxidation through formation and growth of oxide films suggests that the apparent size of metal particles should decrease as a result of metal oxidation. This suggests that the coercive force also should change

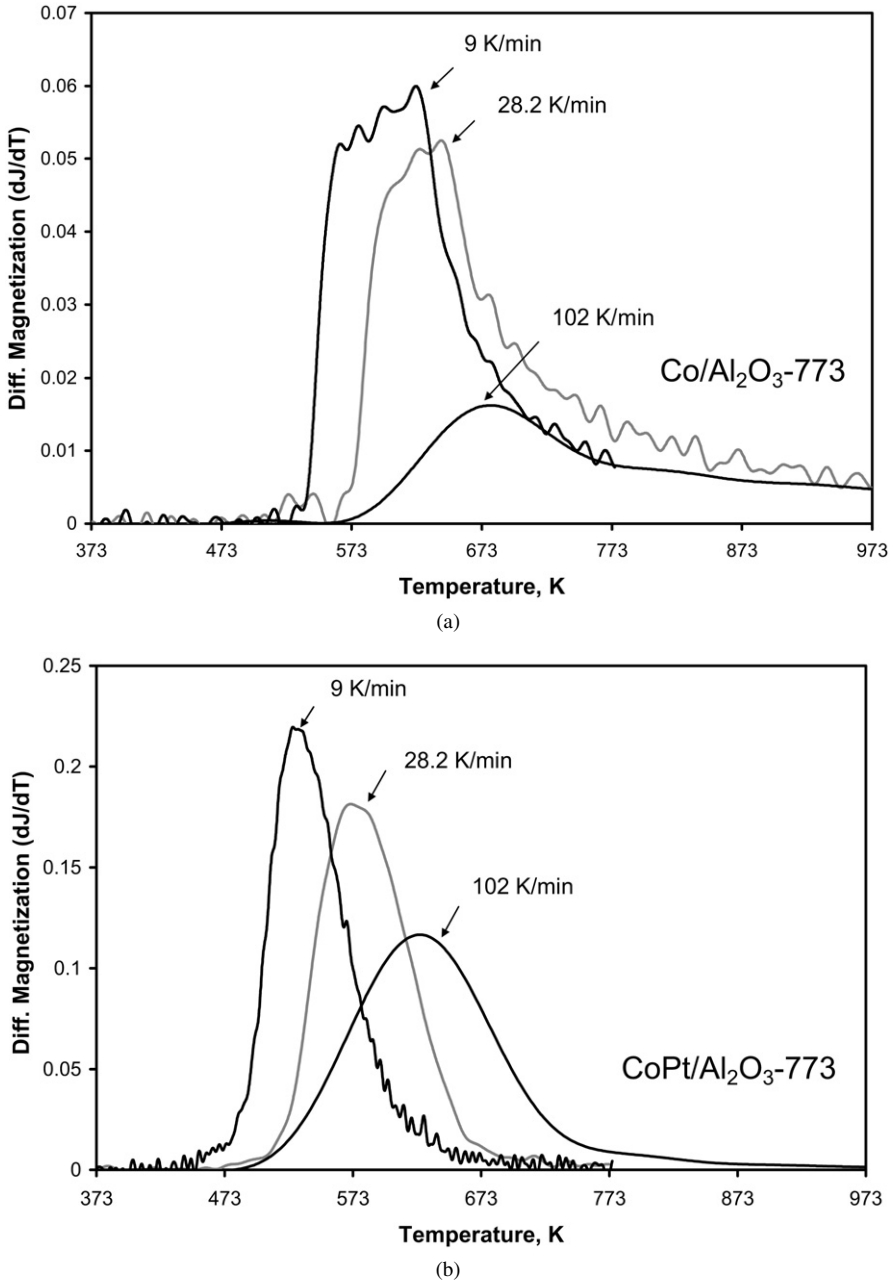

Fig. 8. Influence of temperature rate on the differential magnetization of cobalt monometallic (a) and Pt-promoted (b) alumina-supported catalysts in pure hydrogen.

during oxidation because of the decrease in the apparent cobalt metal particle size. If the catalyst contains cobalt metal particles with an average size >20 nm, then the decrease in cobalt metal particle size during oxidation should lead to an increase in coercive force. If the average size of cobalt particles in the catalysts is <20 nm, cobalt oxidation at lower temperature should produce a decrease in coercive force. Therefore, the average cobalt particle size (< or > 20 nm) in the supported catalysts can be estimated from the variation of coercive force during oxidation at 280 K. For all monometallic and Pt-promoted catalysts in the present work, the coercive force decreased during oxidation in 1%O_2/He mixture at 280 K. This examination showed that the average size of cobalt metal particles was <20 nm in all catalysts studied. Note that this finding is consistent with the data for other characterization techniques. Indeed, Table 1 shows that the cobalt oxide particles were always <20 nm. Cobalt oxide particles are considered precursors of cobalt metal particles.

After the preliminary particle size analysis, the particle size distribution in the catalysts can be evaluated from [48,49]

$$\gamma = 1 - \frac{2J_r}{J_s}, \tag{1}$$

where γ is the fraction of superparamagnetic particles, J_r, is residual magnetization (at zero intensity of magnetic field), and J_s is saturation magnetization. This equation remains valid provided that the catalysts do not contain multidomain ferromagnetic particles ($d > 20$ nm). The upper sizes of cobalt super-

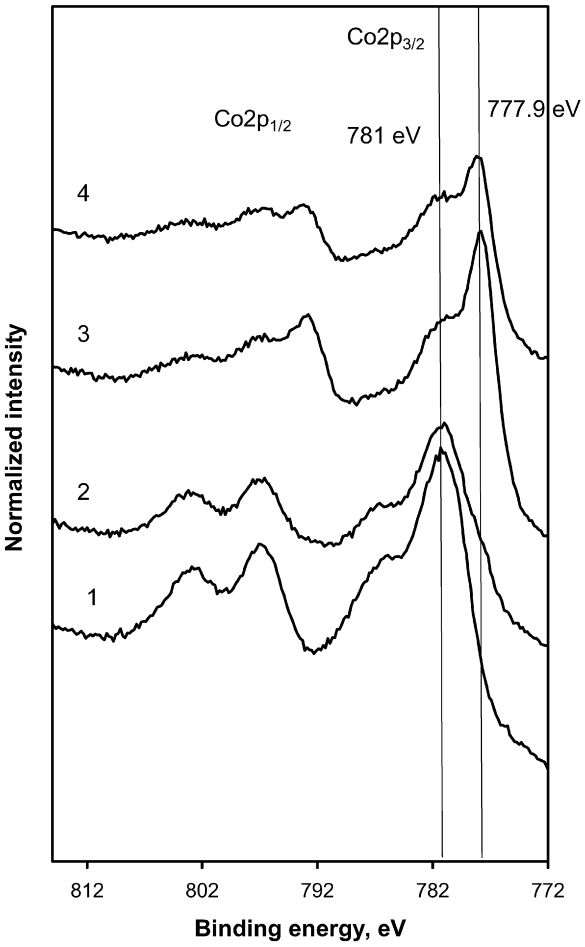

Fig. 9. XPS spectra of Co/Al_2O_3-473 (1), Co/Al_2O_3-613 (2), $CoPt/Al_2O_3$-473 (3), $CoPt/Al_2O_3$-613 (4) after reduction at 673 K in the XPS pre-treatment chamber.

paramagnetic particles can be evaluated from [50,51]

$$KV = 25k_bT, \quad (2)$$

where K is anisotropy constant (for hcp cobalt it is equal to $0.7\ J/cm^3$ [50]), and V is the particle volume. According to this equation, the largest size of cobalt superparamagnetic particles at room temperature was about 7 nm.

Table 3 shows the relative fractions of cobalt superparamagnetic particles determined using Eq. (2) in the catalysts reduced at 673 and 973 K. The fraction of cobalt super paramagnetic particles was about 60–70% in the monometallic catalysts reduced at 673 K, whereas promotion with Pt resulted in a significant increase in the fraction of cobalt superparamagnetic particles (up to 80–90%). The field dependence curves of Pt-promoted cobalt catalysts exhibit smaller coercive force and smaller residual magnetization than those of cobalt monometallic catalysts (Fig. 11). This finding suggests that promotion of cobalt alumina-supported catalysts with platinum resulted in a decrease in the average size of cobalt metal particles. A higher proportion of cobalt superparamagnetic particles was also detected in both cobalt monometallic and Pt-promoted catalysts reduced at 973 K. A more exhaustive interpretation of this phenomenon is given in Section 4.

3.4. Catalytic performance of monometallic and Pt-promoted cobalt alumina-supported catalysts

The catalytic performance of cobalt silica-supported catalysts was evaluated in a differential catalytic reactor at 443–493 K under atmospheric pressure. C1–C20 hydrocarbons and water were the only reaction products under these conditions. The results of catalyst evaluation are summarized in Tables 4 and 5. The FT reaction rates are expressed as cobalt time yields; they were calculated from carbon monoxide conversion, inlet carbon monoxide partial pressure, gas-space velocity, and the amount of cobalt in the reactor.

Relatively low FT rates were observed over monometallic cobalt catalysts. The unpromoted Co/Al_2O_3-473 sample exhibited 2% conversion of carbon monoxide at 453 K and 1800 $cm^3/g/h$ space velocity (Table 4). As expected, carbon monoxide conversion and cobalt time yield increased with the reaction temperature. An increase in the reaction temperature led to a decrease in C5+ and an increase in methane selectivity. The effect of the reaction temperature on methane selectivity was more pronounced for the monometallic cobalt catalyst (Table 4). The apparent Arrhenius activation energy calculated for Co/Al_2O_3-473 from the cobalt time yields (Table 4) was about 80 kJ/mol.

Table 5 shows the effect of catalyst calcination temperature and promotion with Pt on the catalytic performance of a series of cobalt alumina-supported catalysts. With monometallic cobalt catalysts, lower catalytic activity was observed for cobalt catalysts calcined at 473 and 773 K, whereas a slightly higher cobalt time yield was observed for cobalt catalysts pretreated at moderate temperatures (613–673 K). Methane selectivity was about 8% at 463 K, with C5+ selectivity of about 73–77%.

The reaction rates climb very sharply after Pt promotion. With $CoPt/Al_2O_3$-473 K, the conversion of carbon monoxide at 453 K attained a value of 18.4%, which was 8 times higher than with the monometallic Co/Al_2O_3-473 catalyst (Table 5). The methane selectivity increased (from 5.4 to 7.4%) in the Pt-promoted catalysts, and the selectivity to C5+ hydrocarbons decreased from 84 to 79.4% (Tables 4 and 5). After the addition of Pt, the apparent activation energy dropped from 80 to 55 kJ/mol. Similar trends also were observed for cobalt alumina-supported catalysts calcined at higher temperatures (Table 5). Promotion of Co/Al_2O_3-613 with platinum resulted in an increased cobalt time yield from 1.6 to 4.7×10^{-4} mol/cobalt g atom s at 463 K. For Co/Al_2O_3-773, cobalt time yield rose 7-fold, from 0.7 to 5.3×10^{-4} mol/cobalt g atom s. At higher conversion levels, more significant methane and lower C5 selectivities were observed on $CoPt/Al_2O_3$ catalysts (Table 5).

4. Discussion

XPS and X-ray absorption data suggest that in the dried catalysts, cobalt ions have a structural environment similar to that in cobalt nitrate. The EXAFS data revealed no Co–Co coordination. This suggests the presence of only mononuclear cobalt

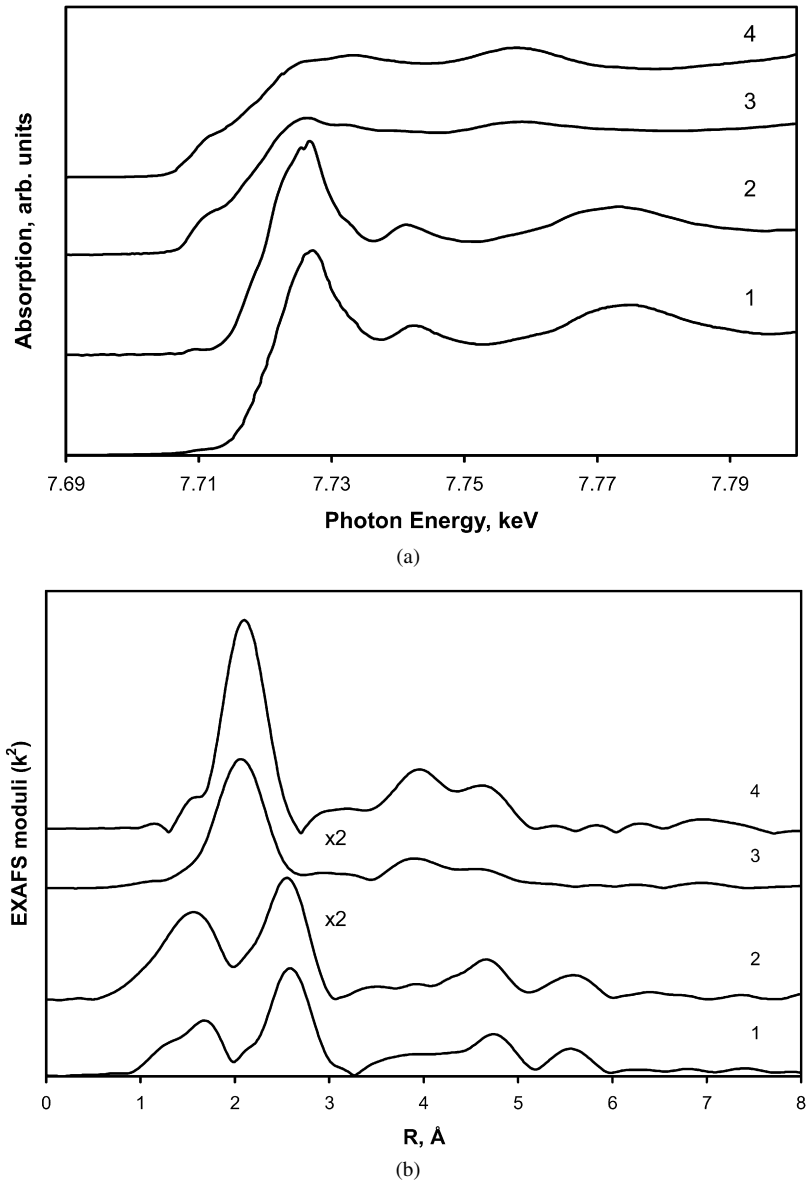

Fig. 10. XANES spectra (a) and k^2-weighted EXAFS Fourier transform moduli (b) for (1) CoO, (2) reduced Co/Al_2O_3-613, (3) reduced $CoPt/Al_2O_3$-613 and (4) metallic cobalt. The reference spectra were measured at room temperature, while the spectra of the catalysts were acquired at 673 K in pure hydrogen.

complexes in the impregnated and dried samples. This result is in agreement with previous data on silica-supported cobalt catalysts [17]. EXAFS detected no polynuclear Co complexes in impregnated and dried monometallic and Ru and Re-promoted Co/SiO_2 catalysts.

Catalyst calcination resulted in decomposition of cobalt nitrate complexes and formation of Co_3O_4 crystallites. The endothermic decomposition of cobalt nitrate proceeded at about 423 K. XPS detected some concentration of nitrogen in the catalysts calcined at 473 K, indicating incomplete decomposition of cobalt nitrate at this temperature. The XRD findings suggest only a slight influence of catalyst calcination temperature on Co_3O_4 crystallite size in both monometallic and Pt-promoted catalysts (Table 1). The XRD data are consistent with XPS measurements. The Co/Al atomic ratios measured using XPS were nearly the same for both monometallic and Pt-promoted cobalt catalysts precalcined at a wide temperature range. Thus, Co_3O_4 particle size does not seem to be significantly affected by either the catalyst calcination temperature or promotion with platinum.

The size of the Co_3O_4 crystallites appeared to be principally limited by alumina pore size. Indeed, the pore sizes of the alumina support were about 8 nm. In all of the catalysts, despite different calcination temperatures and promotion with Pt, Co_3O_4 particle sizes were never larger than 10 nm. This seems to argue in favor of preferential localization of cobalt oxide particles in the pores of alumina, where their sizes are limited by the support pore diameter. Note that the Co_3O_4 particle sizes evaluated from XRD patterns were slightly larger than alumina pore diameters, probably for several reasons [52]. First, the particles of Co_3O_4 could adopt a slightly elongated shape in mesopores. Second, it is known [53] that measuring

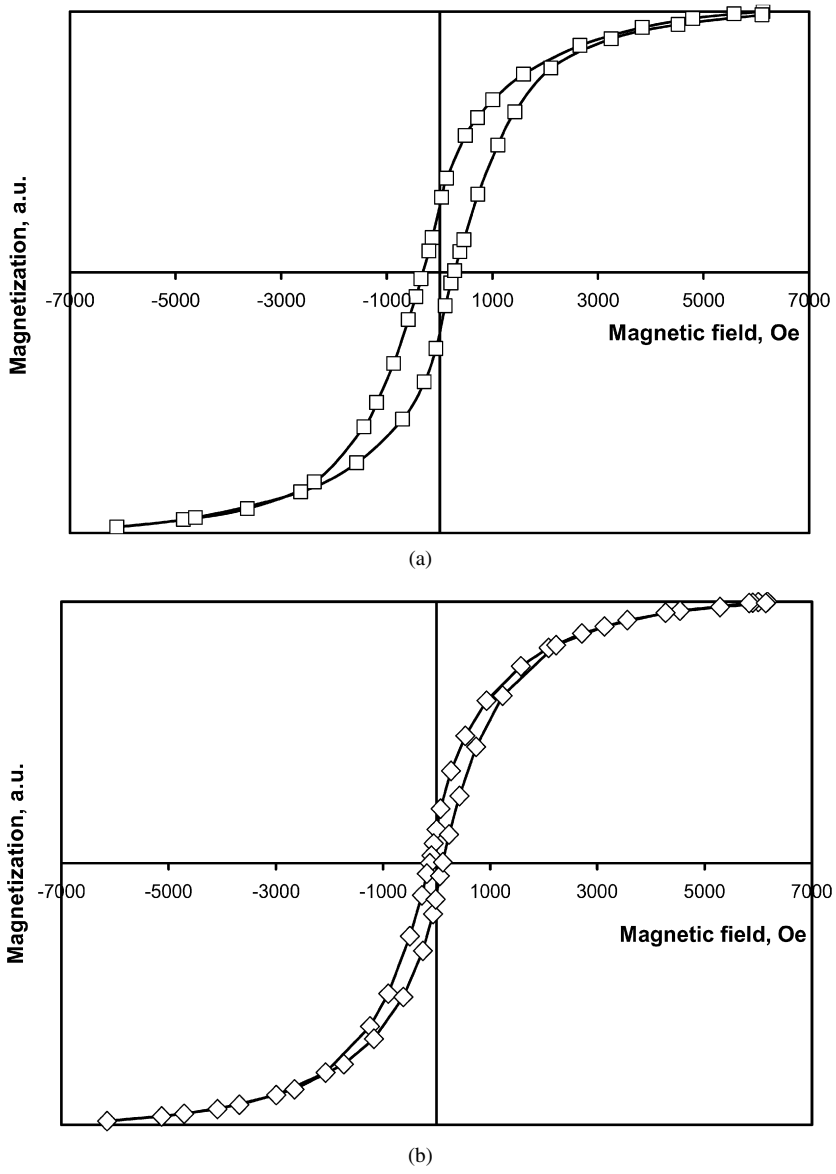

Fig. 11. Field dependence curves for Co/Al_2O_3-773 (a) and $CoPt/Al_2O_3$-773 (b) catalysts reduced at 673 K.

sizes of crystallites from the half-width of the diffraction profile can slightly overestimate crystallite diameters. Third, some very small cobalt particles can be missed by XRD due to significant XRD line broadening. Finally, the presence of small amounts of larger Co_3O_4 particles on alumina outer surface cannot be totally ruled out.

A similar effect of confinement of cobalt oxide particles is consistent with previous findings reported by Holmen [54], Bechara [55], and Xiong [56] for alumina-supported catalysts and our earlier data [15,40,52,57,58] for cobalt catalysts supported by mesoporous silicas. In both cobalt alumina and cobalt silica-supported catalysts, the sizes of cobalt crystallites were strongly affected by pore sizes of the supports. Large cobalt particles are usually found in wider-pore catalysts. It has been found that the support pore diameter produces a more significant effect on the dispersion of cobalt oxide than the overall cobalt content in the catalysts. A more than 10-fold increase in cobalt surface density (0–50 Co/nm^2) did not result in any noticeable sintering of Co_3O_4 particles in SBA-15 periodic mesoporous silicas; the cobalt dispersion seemed to be maintained by the catalyst mesoporous structure. Calcination of both alumina and silica-supported catalysts at temperatures above 673 K resulted in barely reducible cobalt aluminate and cobalt silicate.

The TPR data suggest that cobalt reducibility was affected by catalyst calcination temperature and, most significantly, by promotion with Pt. In monometallic catalysts, the extent of reduction was relatively low. XANES/EXAFS and XPS data show the presence of significant fraction of unreduced cobalt oxides even after extended treatment in hydrogen at 673 K. Fig. 5 shows that TPR peaks shifted to higher temperatures with an increase in the calcination temperature of cobalt monometallic catalysts (from 473 to 773 K). High-temperature shifts of the TPR peaks suggest more difficult reduction of cobalt species. Cobalt reducibility is known to depend on cobalt particle size [38]; smaller cobalt particles are usually much more difficult to reduce than larger ones. More difficult reduction

Table 4
FT catalytic performance of Co/Al_2O_3-473 and $CoPt/Al_2O_3$-473 catalysts at different temperatures

Reaction temperature, K	Conv. CO, %	Cobalt time yield,[a] 10^{-4} mol CO converted/cobalt g atom s	Selectivity (%)			
			CH_4	C_2-HC	C_{3-4}-HC	C_{5+}-HC
Co/Al_2O_3-473						
453	2.2	0.6	5.41	2.78	7.60	84.21
463	3.3	0.9	8.32	4.25	11.71	75.72
473	5.6	1.6	10.87	5.43	14.28	69.42
483	7.9	2.1	20.46	10.31	15.27	53.96
$CoPt/Al_2O_3$-473						
443	12.6	3.5	7.9	3.1	10.1	78.9
448	16.4	4.5	8.0	3.3	10.4	78.3
453	18.4	5.0	7.4	3.6	9.7	79.4
458	20.9	5.7	9.4	4.3	9.6	73.5

Note. Conditions: $P = 1$ bar; 500 mg; GHSV = 1800 $cm^3/g/h$; $H_2/CO = 2$.
[a] Cobalt time yield is the number of moles of converted CO per second divided by the total amount of cobalt (in moles) loaded into the reactor.

of cobalt species in the cobalt monometallic catalysts calcined at higher temperatures cannot be explained simply in terms of varying cobalt particle size; interaction of cobalt oxide with alumina matrix also should be taken into consideration [59,60]. This interaction could be responsible for the more difficult reduction of cobalt catalysts subjected to higher temperatures. Trivalent cobalt and aluminum have rather similar Pauling's ionic radii (0.063 nm for Co^{3+} and 0.054 nm for Al^{3+}). It is known that Co^{3+} of Co_3O_4 can be gradually replaced [61] by Al^{3+} to produce the series of Co_{3-s} Al_sO_4 ($0 < s < 2$) spinels. These series include [62,63] $CoAl_2O_4$, Co_2AlO_4, and Co_3O_4, and more. The interaction between Co_3O_4 and alumina could result in partial substitution of Co^{3+} ions in Co_3O_4 spinel by Al^{3+} ions, thereby hindering the reduction of cobalt species. As expected, higher catalyst calcination temperature and, consequently, incorporation of Al^{3+} ion in Co_3O_4 crystallites resulted (Fig. 5) in higher temperatures of both cobalt oxide reduction steps:

$$Co_3O_4 \rightarrow CoO \rightarrow Co.$$

Cobalt reducibility can be improved considerably by promotion with Pt. The effect of promotion with Pt on cobalt reducibility in alumina-supported FT catalysts is well documented in the literature [64–67]. Our present results are consistent with earlier findings. Fig. 6 shows that in Pt-promoted catalysts, TPR curves exhibit a shifting of hydrogen consumption peaks to lower temperature. The in situ magnetic method also demonstrates lower temperatures of emergence of cobalt metallic phases in the Pt-promoted catalysts. XANES/EXAFS and XPS data also suggest significantly high extent of cobalt reduction in Pt-promoted alumina-supported catalysts (Figs. 9 and 10).

The size of cobalt metal particles in the reduced catalysts was determined using the magnetic method. The fraction of small cobalt superparamagnetic particles was higher in the Pt-promoted catalysts (Table 3). Interestingly, much smaller cobalt metal particles were detected in the Pt-promoted catalysts, whereas XRD and XPS showed almost the same sizes of the parent cobalt oxide particles in the oxidized catalysts. It can be suggested that the presence of Pt led to the reduction of much smaller cobalt oxide particles, whereas only relatively large cobalt oxide particles were reduced in the monometallic catalysts. The small cobalt particles in the monometallic catalysts can be reduced at higher temperatures. Thus, reduction at 973 K decreased the average size of cobalt metal particles (Table 3).

Comparing the characterization and catalytic data provides evidence that the structure of cobalt alumina-supported catalysts had a strong impact on FT catalytic behavior. The cobalt monometallic catalysts exhibited very low FT reaction rates, consistent with the low reducibility of cobalt oxide species. Similar to the dispersion of cobalt oxide, the catalytic performance of alumina-supported cobalt monometallic catalysts is affected only slightly by the catalyst calcination temperature. Promotion with small amounts of Pt, while dramatically enhancing cobalt reducibility, also had a strong influence on FT catalyst performance. A more than 8- to 10-fold increase in the FT reaction rate can be seen; Pt promotion also led to some decrease in C5+ selectivity. It appears that cobalt reducibility is a key issue in the design of efficient cobalt alumina-supported cobalt catalysts prepared using conventional impregnation/calcination.

5. Conclusion

It was found that calcination at 473–773 K temperature range and promotion with small amounts of Pt had no signif-

Table 5
Effect of calcination temperature and promotion with platinum on the catalytic performance of cobalt alumina-supported FT catalysts

Catalyst	Reaction temperature, K	Conversion CO, %	Cobalt time yield, 10^{-4} mol CO converted/cobalt g atom s	Selectivity (%)			
				CH_4	C_2-HC	C_{3-4}-HC	C_{5+}-HC
Co/Al_2O_3-473	453	2.2	0.6	5.4	2.8	7.6	84.2
$CoPt/Al_2O_3$-473	453	18.4	5.0	7.4	3.6	9.7	79.4
Co/Al_2O_3-473	463	3.3	0.9	8.3	4.3	13.7	73.7
Co/Al_2O_3-613	463	5.9	1.6	8.3	3.9	10.6	77.1
$CoPt/Al_2O_3$-613	463	17.2	4.7	10.6	5.1	13.9	70.4
Co/Al_2O_3-673	463	4.6	1.3	8.2	3.9	10.3	77.6
Co/Al_2O_3-773	463	2.7	0.7	6.5	3.6	10.2	79.8
$CoPt/Al_2O_3$-773	463	19.3	5.3	9.6	4.8	13.6	72.1

Note. Conditions: $P = 1$ bar; 500 mg; GHSV = 1800 $cm^3/g/h$; $H_2/CO = 2$.

icant affect the size of Co_3O_4 crystallites in the γ-alumina-supported cobalt FT catalysts. Cobalt dispersion seemed to be influenced primarily by the pore diameter of the support. Cobalt reducibility was relatively low in monometallic cobalt alumina-supported catalysts. The higher calcination temperature of the monometallic cobalt catalysts hindered cobalt reduction. Promotion with 0.1 wt% of platinum resulted in a significantly enhanced cobalt reduction. The presence of platinum seemed to reduce the activation energy of the formation of cobalt metallic phases. Promotion with Pt also favored reduction of smaller Co_3O_4 crystallites and resulted in smaller average sizes of supported cobalt metal particles in the reduced catalysts.

Promotion of cobalt alumina-supported catalysts with small amounts of Pt resulted in a significant increase in the FT reaction rate and some decrease in C5+ hydrocarbon selectivity. The efficient control of cobalt reducibility through calcination and promotion seems to be a key issue in the design of cobalt alumina-supported FT catalysts.

Acknowledgments

Wei Chu thanks the CNRS of France and University of Sciences and Technologies of Lille for providing financial support during his stay as an invited researcher and visiting professor in the Unité de Catalyse et de Chimie du Solide (UMR CNRS 8181). He also acknowledges support from the National Natural Science Foundation of China (NSFC 205903603) and the 985 Project of Sichuan University. Petr A. Chernavskii and Galina A. Pankina acknowledge financial support from the Russian Foundation for Fundamental Research (grant 06-03-32500-a). The authors thank S. Nikitenko, L. Burylo, M. Frère, and O. Gardoll for their help with X-ray absorption, XRD, XPS, DSC–TGA, and TPR measurements and E. Payen, X.Y. Dai, P. Granger, and S. Paul for their help and useful discussions. The European Synchrotron Radiation Facility (ESRF) is acknowledged for the use of synchrotron beam time.

References

[1] M.E. Dry, Catal. Today 71 (2002) 227.
[2] A.Y. Khodakov, W. Chu, P. Fongarland, Chem. Rev. 107 (2007) 1692.
[3] A. Steynberg, M. Dry (Eds.), Fischer–Tropsch Technology, Stud. Surf. Sci. Catal. 152 (2004).
[4] R.L. Espinoza, A.P. Steynberg, B. Jager, A.C. Vosloo, Appl. Catal. A 186 (1–2) (1999) 13.
[5] E. Iglesia, Appl. Catal. A 161 (1997) 59.
[6] E. Iglesia, S.C. Reyes, R.J. Madon, S.L. Soled, Adv. Catal. 39 (1993) 221.
[7] S.L. Soled, E. Iglesia, R.A. Fiato, J.E. Baumgartner, H. Vroman, S. Miseo, Top. Catal. 26 (1–4) (2003) 101.
[8] R.C. Reuel, C.H. Bartholomew, J. Catal. 85 (1984) 78.
[9] A.S. Lisitsyn, A.V. Golovin, V.L. Kuznetsov, Y.I. Yermakov, C1 Mol. Chem. 1 (1984) 115–135.
[10] A.S. Lisitsyn, A.V. Golovin, V.L. Kuznetsov, Y.I. Yermakov, J. Catal. 95 (1985) 527.
[11] G.L. Bezemer, J.H. Bitter, H.P.C.E. Kuipers, H. Oosterbeek, J.E. Holewijn, X. Xu, F. Kapteijn, A.J. van Dillen, K.P. de Jong, J. Am. Chem. Soc. 128 (12) (2006) 3956.
[12] J. van de Loosdrecht, B. Balzhinimaev, J.-A. Dalmon, J.W. Niemantsverdriet, S.V. Tsybulya, A.M. Saib, P.J. van Berge, J.L. Visagie, Catal. Today 123 (2007) 293.
[13] F. Morales, B.M. Weckhuysen, Catal. (R. Soc. Chem.) 19 (2006) 1.
[14] J.-S. Girardon, A.S. Lermontov, L. Gengembre, P.A. Chernavskii, A. Griboval-Constant, A.Y. Khodakov, J. Catal. 230 (2005) 339.
[15] A.Y. Khodakov, J.-S. Girardon, A. Griboval-Constant, A.S. Lermontov, P.A. Chernavskii, Stud. Surf. Sci. Catal. 147 (2004) 295.
[16] J.-S. Girardon, A. Constant-Griboval, L. Gengembre, P.A. Chernavskii, A.Y. Khodakov, Catal. Today 106 (2005) 161.
[17] J.-S. Girardon, E. Quinet, A. Griboval-Constant, P.A. Chernavskii, L. Gengembre, A.Y. Khodakov, J. Catal. 248 (2) (2007) 143.
[18] E. Iglesia, S.L. Soled, J.E. Baumgartner, S.C. Reyes, J. Catal. 153 (1995) 108.
[19] D.I. Enache, B. Rebours, M. Roy-Auberger, R. Revel, J. Catal. 205 (2) (2002) 346.
[20] J. van de Loosdrecht, S. Barradas, E.A. Caricato, N.G. Ngwenya, P.S. Nkwanyana, M.A.S. Rawat, B.H. Sigwebela, P.J. van Berge, J.L. Visagie, Top. Catal. 26 (2003) 121.
[21] J.R.A. Sietsma, J.D. Meeldijk, J.P. Den Breejen, M. Versluijs-Helder, A.J. Van Dillen, P.E. De Jongh, K.P. De Jong, Angew. Chem. Int. Ed. 46 (2007) 4547.
[22] J.R.A. Sietsma, J.P. den Breejen, P.E. de Jongh, A.J. van Dillen, J.H. Bitter, K.P. de Jong, Stud. Surf. Sci. Catal. 167 (2007) 55.
[23] O. Borg, E.A. Blekkan, S. Eri, D. Akporiaye, B. Vigerust, E. Rytter, A. Holmen, Top. Catal. 45 (2007) 39.
[24] B.D. Cullity, Elements of X-Ray Diffraction, Addison–Wesley Publishing Company, London, 1978.
[25] J.-S. Girardon, A.Y. Khodakov, M. Capron, S. Cristol, C. Dujardin, F. Dhainaut, S. Nikitenko, F. Meneau, W. Bras, E. Payen, J. Synchrotron Radiat. 12 (2005) 680.
[26] V.V. Kiselev, P.A. Chernavskii, V.V. Lunin, Russ. J. Phys. Chem. 61 (1987) 151.
[27] P.A. Chernavskii, A.Y. Khodakov, G.V. Pankina, J.-S. Girardon, E. Quinet, Appl. Catal. A 306 (2006) 108.
[28] S.W. Ho, M. Horialla, D.M. Hercules, J. Phys. Chem. 94 (1999) 6396.
[29] T.J. Chaung, C.R. Brundle, D.W. Rice, Surf. Sci. 59 (1976) 413.
[30] T. Cseri, S. Békássy, G. Kenessey, F. Figueras, Thermochim. Acta 288 (1996) 137.
[31] X.Q. Zhao, S. Veintemillas-Verdaguer, O. Bomati-Miguel, M.P. Morales, H.B. Xu, Phys. Rev. B 71 (2005) 024106.
[32] Y. Wang, C.M. Yang, W. Schmidt, B. Spliethoff, E. Bill, F. Schüth, Adv. Mater. 17 (2005) 53.
[33] J.P. Bonnelle, J. Grimblot, A. D'huysser, J. Electron Spectrosc. 7 (1975) 151.
[34] D.G. Castner, P.R. Watson, I.Y. Chan, J. Phys. Chem. 93 (1989) 3188.
[35] G. Jacobs, J.A. Chaney, P.M. Patterson, T.K. Das, J.C. Maillot, B.H. Davis, J. Synchrotron Radiat. 11 (2004) 414.
[36] R. Bechara, D. Balloy, J.-Y. Dauphin, J. Grimblot, Chem. Mater. 11 (1999) 1703.
[37] D.G. Castner, P.R. Watson, I.Y. Chan, J. Phys. Chem. 94 (1990) 819.
[38] A.Yu. Khodakov, J. Lynch, D. Bazin, B. Rebours, N. Zanier, B. Moisson, P. Chaumette, J. Catal. 168 (1997) 16.
[39] B. Ernst, A. Bensaddik, L. Hilaire, P. Chaumette, A. Kiennemann, Catal. Today 39 (1998) 329.
[40] A.Y. Khodakov, A. Griboval-Constant, R. Bechara, F. Villain, J. Phys. Chem. B 105 (2001) 9805.
[41] P.J. Van Berge, J. Van de Loosdrecht, J.L. Visagie, International Patent WO 01/39882 A1, 7 June 2001, assigned to Sasol.
[42] H.E. Kissinger, Anal. Chem. 29 (1957) 1703.
[43] C.H. Bartholomew, Stud. Surf. Sci Catal. 111 (1997) 585.
[44] C.R. Brundle, T.J. Chuang, D.W. Rice, Surf. Sci. 60 (1976) 286.
[45] Y.I. Petrov, Physics of Small Particles, Nauka, Moscow, 1982.
[46] G.V. Pankina, P.A. Chernavskii, V.V. Lunin, Kinet. Catal. 46 (2005) 719.
[47] N. Cabrera, N.F. Mott, Rep. Prog. Phys. 12 (1948–1949) 163.
[48] A. Barbier, A. Hanif, J.-A. Dalmon, G.A. Martin, Appl. Catal. A 168 (1998) 333.
[49] J. Llorca, P. Ramírez de la Piscina, J.-A. Dalmon, J. Sales, N. Homs, Appl. Catal. B 43 (2003) 355.
[50] D.L. Leslie-Pelecky, R.D. Rieke, Chem. Mater. 8 (1996) 1770.
[51] P.A. Chernavskii, Mendeleev Chem. J. XLVI (2002) 19.
[52] A.Y. Khodakov, A. Griboval-Constant, R. Bechara, V.L. Zholobenko, J. Catal. 206 (2002) 230.

[53] P. Ganesan, H.K. Kuo, A. Saaverda, R.J. DeAngelis, J. Catal. 52 (1978) 319.
[54] O. Borg, S. Eri, E.A. Blekkan, S. Storsaeter, H. Wigum, E. Rytter, A. Holmen, J. Catal. 248 (2007) 89.
[55] R. Bechara, D. Balloy, D. Vanhove, Appl. Catal. A 207 (2001) 343.
[56] H. Xiong, Y. Zhang, S. Wang, J. Li, Catal. Commun. 6 (2005) 512.
[57] A.Y. Khodakov, R. Bechara, A. Griboval-Constant, Appl. Catal. A 254 (2003) 273.
[58] A. Griboval-Constant, A.Y. Khodakov, R. Bechara, V.L. Zholobenko, Stud. Surf. Sci. Catal. 144 (2002) 609.
[59] A.A. Khassin, T.M. Yurieva, V.V. Kaichev, V.I. Bukhtiyarov, A.A. Budneva, E.A. Paukshtis, V.N. Parmon, J. Mol. Catal. A 175 (1–2) (2001) 189.
[60] A.A. Khassin, V.F. Anufrienko, V.N. Ikorskii, L.M. Plyasova, G.N. Kustova, T.V. Larina, I.Yu. Molina, V.N. Parmon, Phys. Chem. Chem. Phys. 4 (17) (2002) 4236.
[61] P.G. Casado, I. Rasines, J. Solid State Chem. 52 (1984) 187.
[62] S. Chemlal, A. Larbot, M. Persin, J. Sarrazin, M. Sghyar, M. Rafiq, Mater. Res. Bull. 35 (2000) 2515.
[63] W.S. Cho, M. Kakihana, J. Alloys Compd. 287 (1999) 87.
[64] G.E. Batley, A. Ekstrom, D.A. Johnson, J. Catal. 34 (1975) 368.
[65] L. Guczi, D. Bazin, I. Kovacs, L. Borko, Z. Schay, J. Lynch, P. Parent, C. Lafon, G. Stefler, Z. Koppany, I. Sajo, Top. Catal. 20 (2002) 129.
[66] G. Jacobs, T.K. Das, P.M. Patterson, J. Li, L. Sanchez, B.H. Davis, Appl. Catal. A 247 (2003) 335.
[67] A. Kogelbauer, J.G. Goodwin Jr., R. Oukaci, J. Catal. 160 (1996) 125.